Eocene and Miocene extension, meteoric fluid infiltration, and core complex formation in the Great Basin (Raft River Mountains, Utah)

Methner, K

http://hdl.handle.net/10026.1/8613

10.1002/2014TC003766
Tectonics

AGU PUBLICATIONS

Tectonics

RESEARCH ARTICLE
10.1002/2014TC003766

Key Points:
- Eocene detachment formation predates Miocene Raft River detachment fault
- Localized Eocene and Miocene low δ^2H meteoric fluid infiltration

Supporting Information:
- Text S1 and Table S1–S5

Correspondence to:
K. Methner,
katharina.methner@senckenberg.de

Citation:
Methner, K., A. Mulch, C. Teyssier, M. L. Wells, M. A. Cosca, R. Gottardi, A. Gébelin, and C. P. Chamberlain (2015), Eocene and Miocene extension, meteoric fluid infiltration, and core complex formation in the Great Basin (Raft River Mountains, Utah), *Tectonics*, *34*, doi:10.1002/2014TC003766.

Received 24 OCT 2014
Accepted 24 FEB 2015
Accepted article online 8 MAR 2015

Eocene and Miocene extension, meteoric fluid infiltration, and core complex formation in the Great Basin (Raft River Mountains, Utah)

Katharina Methner[1], Andreas Mulch[1,2], Christian Teyssier[3], Michael L. Wells[4], Michael A. Cosca[5], Raphaël Gottardi[6], Aude Gébelin[1,7], and C. Page Chamberlain[8]

[1]Senckenberg Biodiversity and Climate Research Centre, Senckenberg Research Institute, Frankfurt, Germany, [2]Institute of Geosciences, Goethe University, Frankfurt, Germany, [3]Department of Earth Sciences, University of Minnesota, Twin Cities, Minneapolis, Minnesota, USA, [4]Department of Geoscience, University of Nevada, Las Vegas, Las Vegas, Nevada, USA, [5]U.S. Geological Survey, Denver, Colorado, USA, [6]School of Geosciences, University of Louisiana, Lafayette, Louisiana, USA, [7]School of Geography, Earth and Environmental Sciences, Plymouth University, Plymouth, UK, [8]Environmental Earth System Science, Stanford University, Stanford, California, USA

Abstract Metamorphic core complexes (MCCs) in the North American Cordillera reflect the effects of lithospheric extension and contribute to crustal adjustments both during and after a protracted subduction history along the Pacific plate margin. While the Miocene-to-recent history of most MCCs in the Great Basin, including the Raft River-Albion-Grouse Creek MCC, is well documented, early Cenozoic tectonic fabrics are commonly severely overprinted. We present stable isotope, geochronological (^{40}Ar/^{39}Ar), and microstructural data from the Raft River detachment shear zone. Hydrogen isotope ratios of syntectonic white mica (δ^2H_{ms}) from mylonitic quartzite within the shear zone are very low (−90‰ to −154‰, Vienna SMOW) and result from multiphase synkinematic interaction with surface-derived fluids. ^{40}Ar/^{39}Ar geochronology reveals Eocene (re)crystallization of white mica with $\delta^2H_{ms} \geq -154‰$ in quartzite mylonite of the western segment of the detachment system. These δ^2H_{ms} values are distinctively lower than in localities farther east ($\delta^2H_{ms} \geq -125‰$), where ^{40}Ar/^{39}Ar geochronological data indicate Miocene (18–15 Ma) extensional shearing and mylonitic fabric formation. These data indicate that very low δ^2H surface-derived fluids penetrated the brittle-ductile transition as early as the mid-Eocene during a first phase of exhumation along a detachment rooted to the east. In the eastern part of the core complex, prominent top-to-the-east ductile shearing, mid-Miocene ^{40}Ar/^{39}Ar ages, and higher δ^2H values of recrystallized white mica, indicate Miocene structural and isotopic overprinting of Eocene fabrics.

1. Introduction

Metamorphic core complexes (MCCs) are key elements in understanding the dynamics of lithospheric deformation, mass and heat transfer, and changes in continental topography [e.g., *Coney*, 1980; *Armstrong*, 1982; *Coney and Harms*, 1984; *Dickinson*, 2002; *Mulch et al.*, 2007; *Sullivan and Snoke*, 2007; *Rey et al.*, 2009; *Gébelin et al.*, 2012; *Wells et al.*, 2012; *Whitney et al.*, 2013]. MCCs expose middle to lower crustal rocks and result from denudation and rock uplift through large-scale, low-angle extensional detachment systems. In western North America, MCCs developed during Cenozoic crustal extension and contributed to thermal and mechanical reequilibrium of overthickened orogenic crust following the Sevier orogeny [e.g., *Coney*, 1980; *Wernicke*, 1981; *Armstrong*, 1982; *Coney and Harms*, 1984; *Sonder and Jones*, 1999; *Teyssier et al.*, 2005; *Sullivan and Snoke*, 2007; *Rey et al.*, 2009].

One extensively studied MCC is the Raft River-Albion-Grouse Creek Metamorphic Core Complex (RAG-MCC; NW Utah, USA; Figure 1a) [*Compton et al.*, 1977; *Malavieille*, 1987; *Manning and Bartley*, 1994; *Wells*, 1997, 2001; *Wells et al.*, 1998, 2000, 2004, 2012; *Sheely et al.*, 2001; *Hoisch et al.*, 2002; *Sullivan and Snoke*, 2007; *Gottardi et al.*, 2011, 2015; *Strickland et al.*, 2011a, 2011b; *Konstantinou et al.*, 2012, 2013; *Gottardi and Teyssier*, 2013]. The RAG-MCC records a protracted tectonic history with alternating cycles of Late Cretaceous to Miocene extension and shortening [*Wells*, 1997; *Hoisch et al.*, 2002; *Konstantinou et al.*, 2012; *Wells et al.*, 2012]. Well-documented field evidence indicates that the RAG-MCC hosted at least two major oppositely rooted Cenozoic detachment systems: Eocene/Oligocene and subsequent Miocene extension is manifested in the west-rooted Middle Mountain shear zone (Grouse Creek/Albion Mountains, western RAG-MCC; Figure 1b) [*Saltzer and Hodges*, 1988;

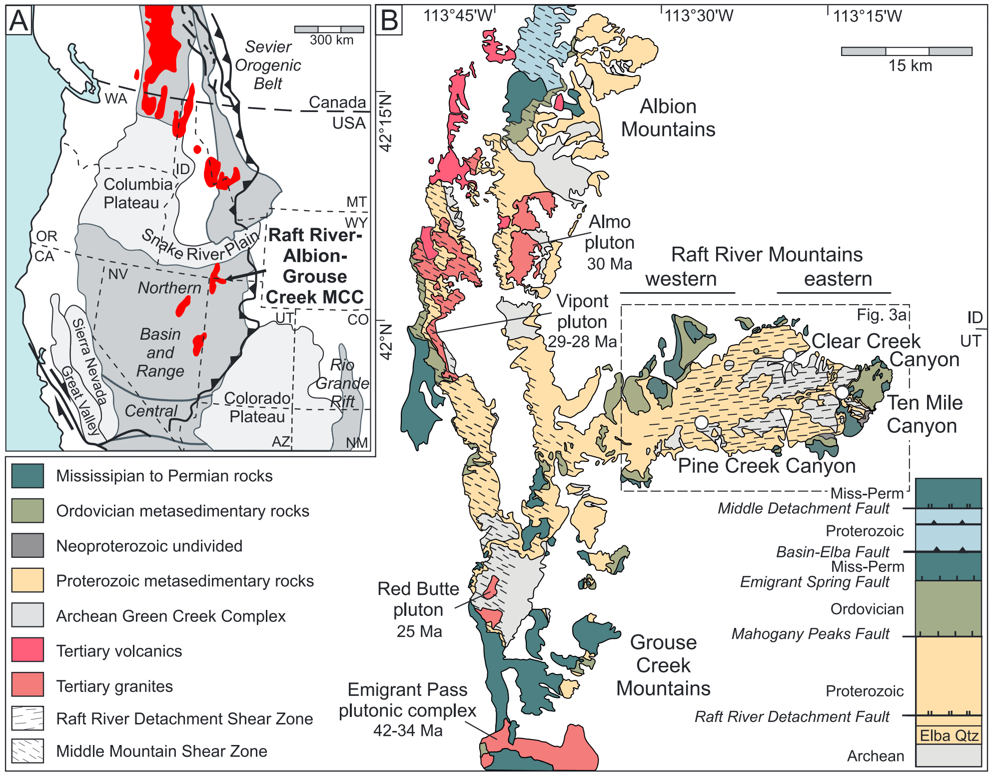

Figure 1. (a) Simplified map of the western United States showing Cenozoic extension (dark grey regions) and metamorphic core complexes (red). Modified from *Foster et al.* [2007] and *Sonder and Jones* [1999], (b) simplified geological map of the Raft River-Albion-Grouse Creek Metamorphic Core Complex with the top-to-the-east Raft River detachment shear zone (RRDSZ) in the Raft River Mountains and the top-to-the-WNW Middle Mountain shear zone in the Albion and Grouse Creek Mountains (modified from *Wells* [1997], *Wells et al.* [2012], and *Konstantinou et al.* [2013]). White dots mark Pine Creek Canyon, Clear Creek Canyon, and Ten Mile Canyon sampling localities.

Wells et al., 2004; *Strickland et al.*, 2011a], whereas the top-to-the-east Raft River detachment shear zone (RRDSZ; Raft River Mountains; eastern RAG-MCC; Figure 1b) is thought to originate from Miocene extensional shearing [*Malavieille*, 1987; *Wells et al.*, 2000; *Wells*, 2001]. As a consequence, reconstructing the crustal response to multiple extension events in the RAG-MCC is challenging owing to tectonic mode switching, reactivation of fault systems, and overprinting of older fabrics by younger tectonic events [e.g., *Miller et al.*, 2012; *Wells and Hoisch*, 2012; *Wells et al.*, 2012].

Localized synextensional interaction of mylonitic footwall rocks with surface-derived fluids is a common feature of extensional detachment systems bounding high-grade MCCs of the western United States [e.g., *Kerrich*, 1988; *Fricke et al.*, 1992; *Wickham et al.*, 1993; *Mulch et al.*, 2004, 2006, 2007; *McFadden et al.*, 2010; *Gottardi et al.*, 2011; *Gébelin et al.*, 2011, 2012, 2014] and has recently been documented in similar environments for other orogens such as the European Alps [*Campani et al.*, 2012], the South Tibetan Detachment [*Gébelin et al.*, 2013], the Alpine Fault [*Menzies et al.*, 2014], or the Menderes MCC [*Hetzel et al.*, 2013]. The infiltration of meteoric water into brittle fault zones and strongly localized fluid flow down to the brittle-ductile transition have been detected mainly by low hydrogen (δ^2H) and oxygen (δ^{18}O) isotope ratios in recrystallized hydrous minerals of mylonitic shear zones [e.g., *Fricke et al.*, 1992; *Wickham et al.*, 1993; *Famin et al.*, 2004; *Mulch et al.*, 2004, 2006]. The δ^2H values of hydrous minerals in otherwise "anhydrous" mylonitic quartzite/silicate rocks have been shown to be a sensitive tracer for fluid-mineral interaction because they are strongly controlled by the D/H ratio of the fluid [e.g., *Mulch et al.*, 2004, 2006; *Mulch and Chamberlain*, 2007]. Muscovite reliably records the δ^2H of the deformation-related fluid flow in detachment shear zones if mineral-fluid isotopic equilibrium is attained and if δ^2H values are preserved over time [e.g., *Mulch et al.*, 2007]. One process that promotes very negative δ^2H values (< -120‰) in formerly high grade metamorphic footwall rocks is the syntectonic interaction with meteoric water [e.g., *Fricke et al.*, 1992; *Wickham et al.*, 1993; *Mulch et al.*, 2004, 2006, 2007; *Mulch and Chamberlain*, 2007].

The presence of surface-derived fluids in such detachment footwall shear zones directly impacts the conditions of crustal flow, mineral recrystallization, elemental and isotopic exchange, and the temperature structure of actively extending crust [e.g., *Morrison and Anderson*, 1998; *Famin et al.,* 2004; *Mulch et al.,* 2006; *Gébelin et al.,* 2011; *Gottardi et al.,* 2011] and is thus one of the primary controls on radiogenic isotope chronometers in extensional shear zones. Therefore, combining stable (δ^2H, δ^{18}O) and radiogenic (^{40}Ar/^{39}Ar) isotope with microstructural analyses provides insight into the timing of detachment-controlled fluid flow and allows the links between fault-related fluid-rock interaction and the rapid temporal and kinematic evolution of extensional detachment zones to be studied [e.g., *Mulch et al.,* 2004, 2005; *Mulch and Chamberlain*, 2007; *Person et al.,* 2007].

Here we present δ^2H, δ^{18}O, ^{40}Ar/^{39}Ar geochronological, and microstructural data from exhumed mylonitic footwall rocks of the RRDSZ that directly underlies the detachment fault. These data were collected on a ~20 km long E-W transect approximately along the shear direction to assess the deformation and time-integrated fluid flow history of the RRDSZ. Three observations characterize these combined data sets: (1) minimum δ^2H values in syntectonically recrystallized muscovite (δ^2H_{ms}) in the western Raft River Mountains are distinctively lower (-154‰) than the δ^2H_{ms} values in Miocene quartzite mylonite from the eastern localities (-122‰ to -125‰), (2) ^{40}Ar/^{39}Ar geochronology reveals that recrystallization and resetting of low-δ^2H white mica occurred during Eocene extensional deformation in the western Raft River Mountains, and (3) the spatial pattern of δ^2H_{ms} values across a vertical footwall section in the western Raft River Mountains suggests that E-directed Miocene overprint along the RRDSZ created new pathways for meteoric fluids at different levels within the Eocene (circa 45–40 Ma) quartzite fabric. We propose that exhumation along the Eocene RRDSZ was accompanied by infiltration of very low δ^2H meteoric fluids (δ^2H_{fluid} as low as -126‰). During mid-Miocene (Basin and Range) extension and meteoric fluid infiltration (δ^2H_{fluid} as low as -103‰) the highest strain developed in the eastern Raft River Mountains. Miocene shearing reactivated preexisting fabrics along the RRDSZ in the western Raft River Mountains, inducing strongly localized hydrogen isotope exchange in deforming white mica.

2. The Raft River-Albion-Grouse Creek Metamorphic Core Complex

The RAG-MCC is located in the hinterland of the Sevier orogenic belt (Figure 1a) [e.g., *Armstrong*, 1968; *Dickinson*, 2002; *DeCelles*, 2004; *Sullivan and Snoke*, 2007]. Previous studies have proposed diverse kinematic histories including Mesozoic crustal shortening and synconvergent extension followed by multiple episodes of Cenozoic extension [*Wells*, 1997; *Wells et al.,* 1998, 2012; *Hoisch et al.,* 2002; *Konstantinou et al.,* 2012] along two oppositely directed detachment systems, which were synchronously active for at least part of their history [*Malavieille*, 1987; *Wells et al.,* 2000; *Sullivan and Snoke*, 2007]. The top-to-the-WNW Middle Mountain shear zone located in the Albion, Grouse Creek, and western Raft River Mountains is a long-lived, amphibolite-facies extensional shear zone of middle-late Eocene to Oligocene age (Figure 1b) [*Saltzer and Hodges*, 1988; *Wells et al.,* 2004; *Strickland et al.,* 2011a] that was reactivated during the Oligo-Miocene [*Sheely et al.,* 2001] following the intrusion of synextensional, late Eocene to Oligocene plutons [*Compton et al.,* 1977; *Egger et al.,* 2003; *Strickland et al.,* 2011b; *Konstantinou et al.,* 2012, 2013]. The top-to-the-east Miocene Raft River detachment and its underlying detachment shear zone (RRDSZ) are best exposed at the Ten Mile and Clear Creek Canyon localities in the eastern Raft River Mountains (Figure 1b) [e.g., *Malavieille*, 1987; *Wells et al.,* 2000; *Wells*, 2001]. Along this detachment fault, upper plate rocks of Neoproterozoic to Paleozoic age are displaced by up to 30 km against Archean to Proterozoic footwall rocks [*Compton et al.,* 1977]. Beneath the detachment fault, rocks within the 50 to 300 m thick RRDSZ have been extensively mylonitized and metamorphosed under greenschist-facies conditions [*Compton et al.,* 1977; *Wells*, 1997, 2001; *Wells et al.,* 2000]. They are characterized by a subhorizontal foliation and a regional east-west directed stretching lineation [e.g., *Compton*, 1980; *Malavieille*, 1987; *Wells,* 1997, 2001]. Mica ^{40}Ar/^{39}Ar ages become younger from the western (~47 Ma) to the eastern Raft River Mountains (~15 Ma) and have been interpreted as cooling ages [*Wells et al.,* 2000]. When considered together with apatite fission-track ages, the combined geochronological data reveal a pattern of protracted, extension-induced cooling and unroofing history along the RRDSZ and the overlying detachment fault [*Wells et al.,* 2000].

3. Results

In the following we report microstructural, ^{40}Ar/^{39}Ar geochronological, and hydrogen (δ^2H) and oxygen (δ^{18}O) isotopic data from three sections of Elba Quartzite located in the western (Pine Creek Canyon) and eastern (Clear Creek Canyon and Ten Mile Canyon) Raft River Mountains (Figure 1b).

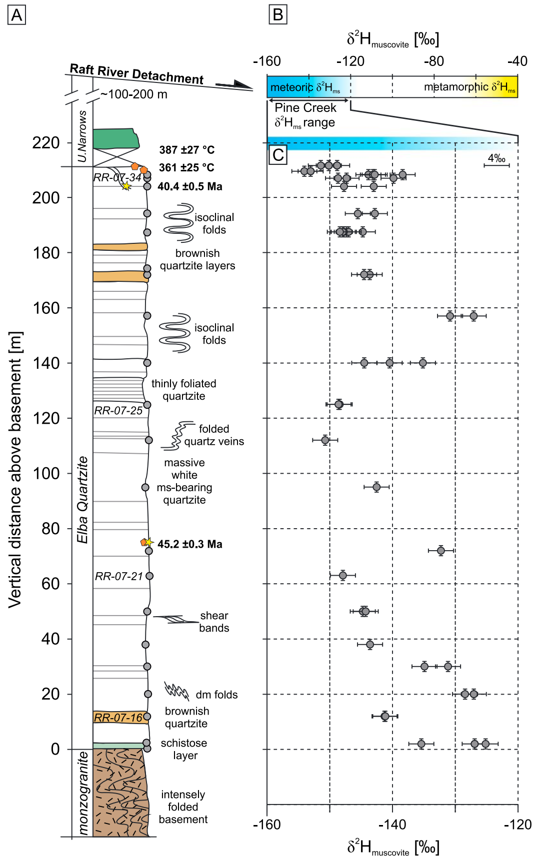

Figure 2. (a) Section of variably deformed Elba Quartzite at Pine Creek Canyon showing the location of hydrogen isotope (circles), $^{40}Ar/^{39}Ar$ geochronology (stars), and oxygen isotope exchange thermometry (pentagons) samples. (b) Range of typical δ^2H_{ms} values indicative of interaction with meteoric and metamorphic fluids (notice the different scale compared to Figure 2c). (c) Muscovite hydrogen isotope values (δ^2H_{ms}) of Elba Quartzite at Pine Creek Canyon. Multiple data points show replicates and different grain size fractions.

At Pine Creek Canyon, rocks in the footwall of the Raft River detachment comprise late Archean basement (~2.5 Ga gneissic monzogranite) unconformably overlain by Neoproterozoic metasedimentary rocks, which include the approximately 200 m thick Elba Quartzite composed of quartz and white mica and the overlying schist of Upper Narrows (Figure 2a) [*Compton et al.,* 1977; *Wells*, 2001]. Footwall rocks from Pine Creek Canyon experienced cooling below ~400°C in the early to middle Eocene (47 to 44 Ma), followed by a second phase of rapid cooling starting at about 16 Ma [*Wells et al.,* 2000; *Harrison et al.,* 2009].

A strong increase in strain intensity from west to east along the RRDSZ is responsible for the substantial eastward thinning of Elba Quartzite (Figure 3) [*Wells*, 2001; *Sullivan*, 2008]. Middle Miocene (16–13 Ma) cooling and exhumation is best documented in the eastern Raft River Mountains. Here the Clear Creek Canyon section (Figures 1b, 3a, and 3c) exposes an approximately 100 m thick section of the RRDSZ, comprising monzogranitic basement and overlying Elba Quartzite. The Elba Quartzite includes from bottom to top: (1) a basal quartzite cobble metaconglomerate, (2) an interval of white quartzite and muscovite-quartzite schist, (3) a distinct layer of red quartzite, and (4) a pebble metaconglomerate [*Sullivan*, 2008; *Gottardi et al.,* 2011; *Gottardi and Teyssier*, 2013]. Mylonitic foliation in the Elba Quartzite dips gently to the NE, and mineral lineation is E-trending and gently plunging [*Sullivan*, 2008]. The structurally deepest exposure of the RRDSZ Elba Quartzite is at Ten Mile Canyon (Figures 1b, 3a, and 3d), where the ~60 m thick section comprises, from bottom to top, Archean basement, muscovite-kyanite schist (15 m), white Elba Quartzite and a layer of reddish Elba Quartzite (35 m), and the overlying schist member of the Elba Quartzite (11 m) [*Wells et al.,* 2000].

3.1. Western Raft River Mountains: Pine Creek Canyon

We systematically sampled 210 m of Elba Quartzite with a sample spacing of about 10 m covering the complete section from the top of the Archean basement to the schist unit overlying the quartzite (Figure 2a). All sampled rocks display a well-developed subhorizontal (mylonitic) foliation and a prominent E-W to ESE-WNW trending stretching lineation (Figures 4a and 4b).

3.1.1. Microstructure

Elba Quartzite at Pine Creek Canyon consists almost entirely of quartz and white mica (5–15%) with only minor amounts of accessory minerals (e.g., Figure 4c). Elongate muscovite grains with high aspect ratios are arranged in small bands and trails and define the subhorizontal foliation (C-surfaces) (Figure 4c). Shape preferred orientation (SPO) of quartz grains defines an oblique foliation with respect to white mica grains, with an angle that decreases from 30 to 40° at the top of the section to $< 5°$ when approaching the contact with the underlying basement. The SPO in relation to the C-surfaces defines shear bands and indicates top-to-the-east shearing (Figure 4c) [*Simpson and Schmid*, 1983; *Lister and Snoke*, 1984].

In quartz grain boundary migration recrystallization was dominant as revealed by pinning effects on quartz grain boundaries, castellate quartz grain boundaries, inclusion of small mica grains within quartz, and

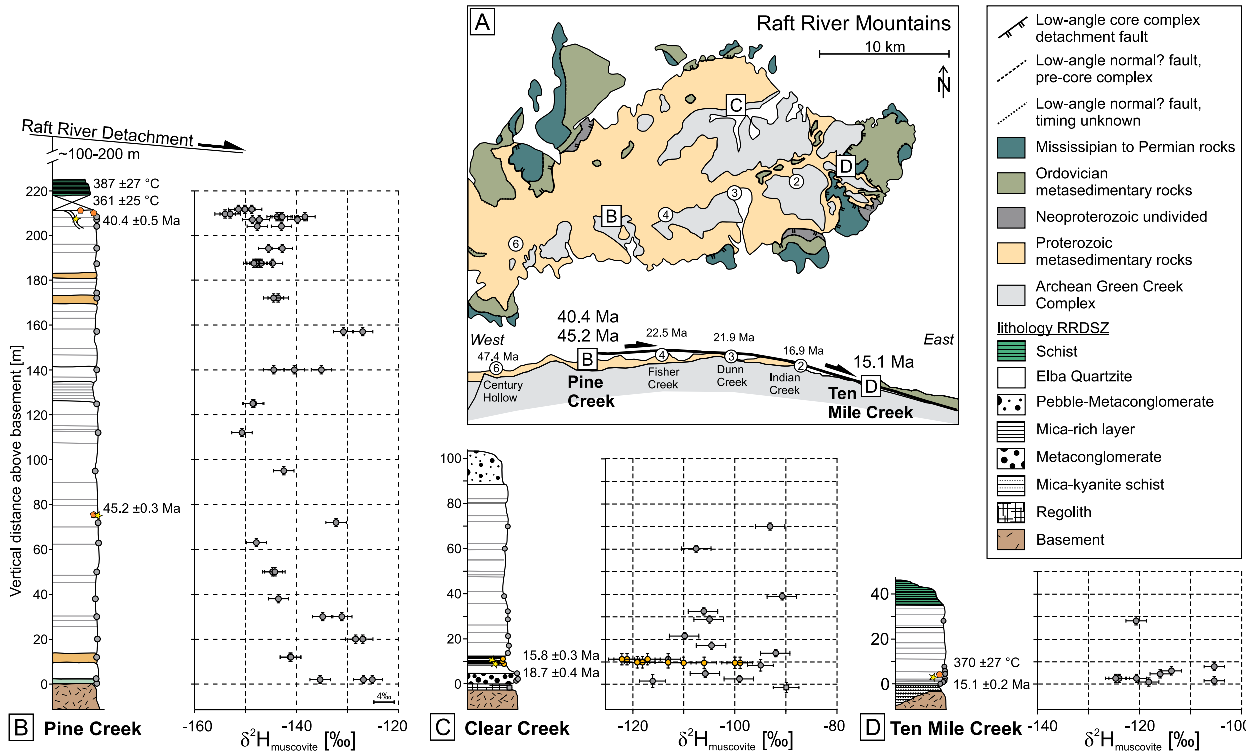

Figure 3. (a) Simplified geological map and cross section of the Raft River Mountains (with sampling localities: B = Pine Creek Canyon, C = Clear Creek Canyon, and D = Ten Mile Creek) adapted from *Wells et al.* [2000]. (b–d) Sections through Elba Quartzite with δ^2H_{ms} values (versus VSMOW) from mylonitic quartzite (grey circles), mica-rich schist (orange circles), regolith (grey square), oxygen exchange-based temperatures (orange pentagons), and $^{40}Ar/^{39}Ar$ data (yellow stars) from each sampling locality: (Figure 3b) Pine Creek Canyon, (Figure 3c) Clear Creek Canyon, and (Figure 3d) Ten Mile Creek Canyon. The composite section as well as δ^2H_{ms} values from mylonitic quartzite (grey circles) of the Clear Creek Canyon are adapted from *Gottardi et al.* [2011]. The succession of profiles from west to east reveals the thinning of the Elba Quartzite in the direction of shearing.

alignment of fluid inclusions along quartz grain boundaries owing to dragging effects (Figures 4c–4e) [*Jessell*, 1987; *Drury and Urai*, 1990]. Internal deformation features such as undulose extinction, subgrains, and deformation lamellae are common in larger quartz grains (Figure 4e). Sutured grain boundaries and small grain boundary bulges (Figure 4d) indicate minor recrystallization by local grain boundary bulging [e.g., *Stipp et al.*, 2002] with preferred bulging sites approximately normal to the subhorizontal foliation. These higher strain layers alternate with quartzite layers that lack evidence for low-temperature deformation microstructures and preserve higher temperature grain boundary migration recrystallization microstructures (Figure 4f).

3.1.2. $^{40}Ar/^{39}Ar$ Geochronology

Using laser step-heating $^{40}Ar/^{39}Ar$ geochronology, we dated muscovite from a deformed and recrystallized syntectonic muscovite-bearing quartz vein that cuts the mylonitic quartzite at the top of the Pine Creek Canyon section (Figure 5a; sample RR-04-123; for methods and data, see supporting information). Field observation suggests that the deformed vein is synmylonitic to late-mylonitic, as it is still rather coarse grained and cuts the mylonitic foliation at high angle. The $^{40}Ar/^{39}Ar$ release spectrum from degasing of two grains defines a plateau-like segment with an age of 40.4 ± 0.5 Ma (weighted mean age, ~70% of ^{39}Ar released); low-temperature increments show apparent ^{40}Ar loss (Figure 5a). Despite similar ^{39}Ar release patterns (Figure 5a) this incremental heating $^{40}Ar/^{39}Ar$ age is somewhat younger than the muscovite $^{40}Ar/^{39}Ar$ age of 45.2 ± 0.3 Ma obtained by furnace heating of milligram quantities of fabric-forming muscovite (RR91-20) in the deeper levels (~75 m) of the Elba Quartzite of Pine Creek Canyon [*Wells et al.*, 2000].

3.1.3. Hydrogen and Oxygen Isotope Geochemistry

δ^2H_{ms} values from 22 Elba Quartzite samples are very low and range from −125‰ to −154‰ (VSMOW; Figures 2b and 3b; for methods and data, see supporting information). Overall, we observe two characteristics in the δ^2H_{ms} values: (1) from bottom to top of the section, minimum δ^2H_{ms} values decrease from −141‰ to −154‰; and (2) four intervals (at 0 m, 20 m, 75 m, and 157 m, respectively) display locally increasing δ^2H_{ms} values reaching maximum values between −132‰ and −125‰ (Figure 2b).

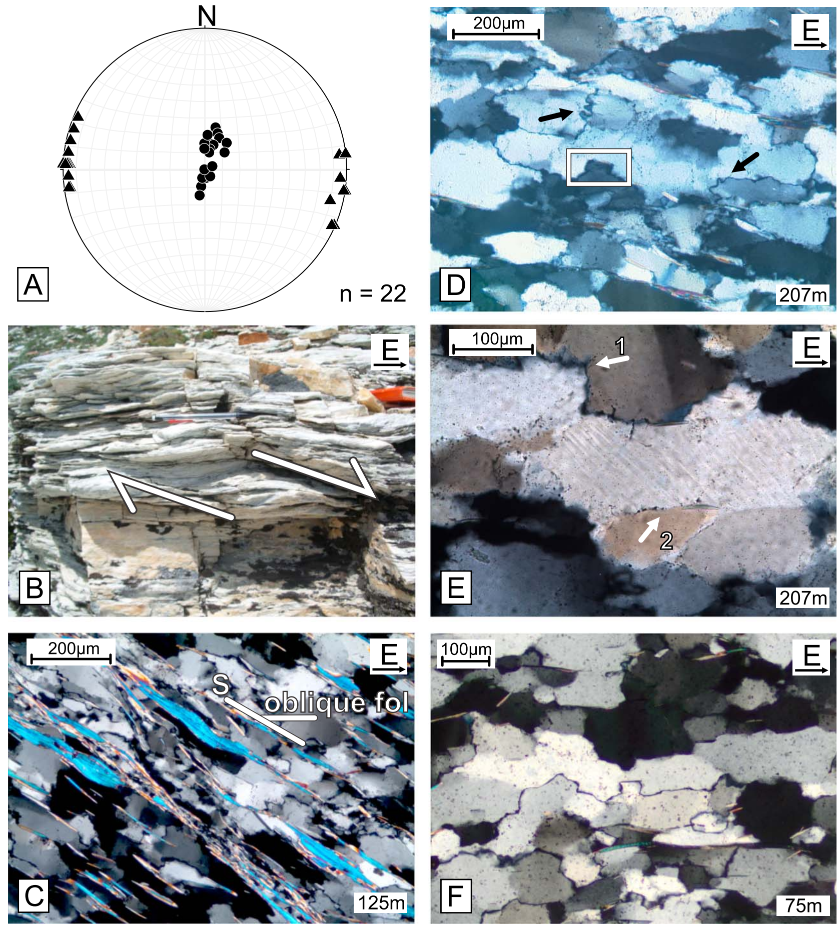

Figure 4. Macroscopic and microscopic structures of the deformed Elba Quartzite at Pine Creek Canyon: (a) Stereogram of foliation poles (circles) and stretching lineation (triangles). (b) Mylonitic foliation with C′-shear bands indicating top-to-the east sense of shear. (c) Flat and elongate muscovite parallels C-plane with very high aspect ratios; grain-size reduction of quartz occurs preferentially in mica-rich parts (RR-07-25, 125 m above basement). (d) Grain boundary bulging and migration at the boundaries of large quartz grains (arrows) and castellated grain shape of quartz (box) (RR-07-34, 207 m). (e) Deformation lamellae indicative of high differential stress in large quartz grains (RR-07-34, 207 m). Castellate grain boundaries (arrow 1) and grain boundary pinning as well as aligned fluid inclusions (arrow 2) point to mobile grain boundaries. (f) Elba Quartzite sample with high-temperature grain boundary migration recrystallization microstructures, lacking evidence for low-temperature deformation microstructures such as grain boundary bulging, deformation bands, deformation lamellae, or undulose extinction (RR91-20, 75 m).

In general, such low δ^2H_{ms} values (−125‰ to −154‰) indicate hydrogen isotope exchange with fluids of meteoric origin that penetrated into the active hanging wall-footwall interface and affected δ^2H values of recrystallizing muscovite [e.g., *Taylor*, 1978; *Sheppard*, 1986; *Kerrich*, 1988; *Wickham et al.*, 1993; *Mulch et al.*, 2007].

Three samples of Elba Quartzite were analyzed for $\delta^{18}O$ values of quartz ($\delta^{18}O_{qtz}$) and muscovite ($\delta^{18}O_{ms}$) (Figure 2a and supporting information). Two of the three samples (RR-04-121 and RR-04-125c) indicate oxygen isotope equilibrium, with quartz and muscovite $\delta^{18}O$ values of 11.7‰ and 8.5‰ (RR-04-121; 211 m) and 11.2‰ and 7.7‰ (RR-04-125c; 209 m), respectively. Equilibrium oxygen isotope fractionation between quartz and muscovite ($\Delta^{18}O_{qtz\text{-}ms}$) is temperature dependent and exchange temperatures can be calculated provided that oxygen isotope equilibrium between the two mineral phases was attained during recrystallization. Using the calibration of *Chacko et al.* [1996], $\Delta^{18}O_{qtz\text{-}ms}$ values of 3.2‰ (RR-04-121) and 3.5‰ (RR-04-125c) translate into exchange temperatures of 387 ± 27°C and 361 ± 25°C, respectively. These $\delta^{18}O_{qtz}$ and $\delta^{18}O_{ms}$ values are significantly lower (1.3 to 1.8‰ in $\delta^{18}O_{qtz}$ and 3.8 to 4.6‰ in $\delta^{18}O_{ms}$) than those of sample RR91-20 (with $\delta^{18}O_{qtz}$ = 13.0‰ and $\delta^{18}O_{ms}$ = 12.3‰; at 75 m in Figure 2a) dated at 45.2 ± 0.3 Ma [*Wells et al.*, 2000].

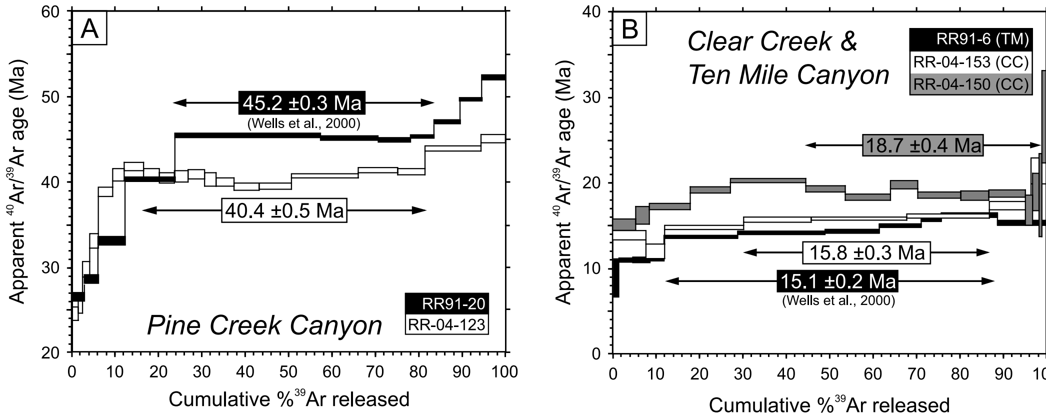

Figure 5. $^{40}Ar/^{39}Ar$ age spectra of white mica from (a) Pine Creek Canyon and (b) Clear Creek Canyon (CC) and Ten Mile Canyon (TM) localities. Black spectra are bulk furnace heating results [*Wells et al.,* 2000], white and grey spectra are laser heating experiments of 2–4 grains (this study). Results from samples of this study do not form $^{40}Ar/^{39}Ar$ plateau ages by any standard criteria, rather preferred weighted mean ages for each sample are reported from contiguous incremental heating steps with > 50% of ^{39}Ar released that have similar $^{40}Ar^*/^{39}Ar$ ratios.

The resulting low $\Delta^{18}O_{qtz\text{-}ms} = 0.7‰$ value yields unrealistic temperatures (>1100°C) and thus points to nonequilibrium oxygen isotope fractionation in this sample.

3.2. Eastern Raft River Mountains: Clear Creek Canyon

3.2.1. Microstructure

Elba Quartzite exhibits a well-developed mylonitic foliation and lineation both defined by elongated quartz and white mica grains. Quartz grains are coarse (>1000 µm long) elongated ribbons that commonly display strong undulose extinction, deformation bands, and deformation lamellae, or finer recrystallized grains (50–100 µm) along grain boundaries that resulted mainly from subgrain rotation recrystallization [see also *Wells,* 2001; *Sullivan,* 2008; *Gottardi et al.,* 2011; *Gottardi and Teyssier,* 2013]. Oblique secondary foliation of recrystallized quartz grains [*Gottardi et al.,* 2011] and shear bands in muscovite-quartz schist units [*Sullivan*, 2008] consistently indicate top-to-the-east sense of shear. At Clear Creek Canyon, the Elba Quartzite also recorded a significant component of coaxial deformation [*Wells*, 2001; *Sullivan*, 2008], which is supported by electron backscatter diffraction analysis showing type-I cross girdles of quartz *c* axes and nearly symmetrical *a* axis maxima [*Gottardi et al.,* 2011; *Gottardi and Teyssier*, 2013].

3.2.2. $^{40}Ar/^{39}Ar$ Geochronology

Muscovites from a deformed muscovite-bearing quartz vein in strongly veined quartzite (RR-04-150) and a white mica-rich schist layer within the quartzite (RR-04-153) from the base of the RRDSZ were dated by laser step heating $^{40}Ar/^{39}Ar$ geochronology (Figure 3c and see supporting information). Both $^{40}Ar/^{39}Ar$ release spectra were obtained by incrementally heating four muscovite grains, and each sample defines plateau-like segments over 45–98% (RR-04-150) and 30–85% (RR-04-153) of ^{39}Ar released, with calculated weighted mean ages of 18.7 ± 0.4 Ma and 15.8 ± 0.3 Ma, respectively (Figure 5b).

3.2.3. Hydrogen and Oxygen Isotope Geochemistry

δ^2H_{ms} values of (a) metamorphosed regolith at the very top of the Archean basement (−2 to 0 m), (b) muscovite-rich layers of the metaconglomerate (0 to 5 m), and (c) distinct layers of muscovite-quartz schist (5 to 70 m) range from −90‰ to −122‰ (Figure 3c and supporting information). δ^2H_{ms} values are highest in the metamorphosed muscovite-rich regolith (−90‰) and decrease rapidly by about 25‰ (from −95‰ to −122‰) within the quartz-muscovite schist layer at the base of the RRDSZ. The range of δ^2H_{ms} values encompasses previously determined δ^2H_{ms} values of mylonitic muscovite-bearing quartzite from Clear Creek Canyon [*Gottardi et al.,* 2011], and the combined data set reveals δ^2H_{ms} values that are significantly higher ($\delta^2H_{ms} = -90$ to −122‰) than those from the Pine Creek Canyon quartzite ($\delta^2H_{ms} = -125‰$ to −154‰), but still far below the δ^2H_{ms} range ($\delta^2H_{ms} = -50‰$ to −70‰) typically encountered in metamorphic rocks (Figure 2b) [e.g., *Taylor*, 1978; *Sheppard*, 1986; *Kerrich*, 1988; *Wickham et al.,* 1993].

Oxygen isotope exchange thermometry at Clear Creek Canyon [*Gottardi et al.,* 2011] indicates a steep geothermal gradient with temperatures increasing from 345 ± 25°C at the top to 485 ± 20°C near the base of the 100 m thick RRDSZ and a diverse pattern of fluid flow and fluid-rock interaction that responds to changes from flattening to constrictional strain along the shear zone [*Gottardi et al.,* 2015].

3.3. Eastern Raft River Mountains: Ten Mile Canyon

3.3.1. Microstructure

Rocks from Ten Mile Canyon record the highest strains and strongest thinning of Elba Quartzite along the RRDSZ [*Wells et al.,* 2000]. In thin section, quartzite shows highly elongate quartz ribbons with aspect ratios >40 and lengths commonly >2000 μm and variable degrees of recrystallization and recovery. Relict ribbons are characterized by domains of newly recrystallized grains of ~20 μm diameter that commonly show an oblique SPO consistent with top-to-the-east shear and a strong lattice-preferred orientation. Other ribbons show internal mosaics of subgrains of similar size to newly recrystallized grains. Quartz microstructures are consistent with dynamic recrystallization by subgrain rotation recrystallization [e.g., *Stipp et al.,* 2002]. Feldspar lacks evidence for crystal plasticity and is commonly fractured at high angles to foliation.

3.3.2. $^{40}Ar/^{39}Ar$ Geochronology

Bulk muscovite $^{40}Ar/^{39}Ar$ ages of 15.05 ± 0.18 Ma (RR91-6, mylonitic quartzite [*Wells et al.,* 2000]) and 14.88 ± 0.17 Ma (RR91-7, quartz-muscovite-kyanite schist [*Wells et al.,* 2000]), combined with biotite $^{40}Ar/^{39}Ar$ and zircon fission-track thermochronology, indicate an age range of ~16 Ma to ~10 Ma for ductile and subsequent brittle extensional shearing at the Ten Mile Canyon locality, while the Pine Creek locality had already cooled through the $^{40}Ar/^{39}Ar$ muscovite and biotite closure temperature interval prior to Miocene extension [*Wells et al.,* 2000].

3.3.3. Hydrogen and Oxygen Isotope Geochemistry

δ^2H_{ms} values of muscovite-bearing mylonitic quartzite and schist from Ten Mile Canyon range from −106‰ to −125‰ with no systematic spatial relationship across the mylonitic shear zone (Figure 3d and supporting information). Similar to the Clear Creek Canyon locality, δ^2H_{ms} values are (1) low when compared to typical metamorphic mineral assemblages that interacted with metamorphic fluids [e.g., *Sheppard*, 1986] and (2) clearly influenced by interaction with meteoric fluids at elevated temperatures (350–400°C) but (3) significantly higher than δ^2H_{ms} values from Pine Creek Canyon in the western Raft River Mountains.

Analysis of one mylonitic quartzite sample (RR100-89, supporting information) yielded $\delta^{18}O$ values of quartz and muscovite of $\delta^{18}O_{qtz}$ = 12.3‰ and $\delta^{18}O_{ms}$ = 8.8‰. Quartz-muscovite oxygen isotope fraction, $\Delta^{18}O_{qtz\text{-}ms}$ = 3.5‰, is consistent with deformation temperatures of 370 ± 27°C [*Chacko et al.,* 1996].

4. Discussion

Our combined microstructural, δ^2H, $\delta^{18}O$, and $^{40}Ar/^{39}Ar$ geochronologic data point to Eocene (45–40 Ma) and Miocene (18–15 Ma) phases of extension along the RRDSZ, each characterized by similar temperature conditions, yet under the presence of meteoric fluids with strikingly different δ^2H values.

4.1. $^{40}Ar/^{39}Ar$ Geochronology and Timing of Deformation

Interpretation of $^{40}Ar/^{39}Ar$ ages in recrystallized rocks that were deformed within the closure temperature interval for ^{40}Ar diffusion is challenging [e.g., *Mulch and Cosca*, 2004; *Harrison et al.,* 2009; *Cosca et al.,* 2011], yet combined isotopic and elemental tracer data can provide additional insight into the ^{40}Ar retention behavior especially for white mica in ductile shear zones [e.g., *Mulch et al.,* 2005, 2006; *Gébelin et al.,* 2011; *Cosca et al.,* 2011]. The fact that the individual sections across the RAG-MCC preserve distinct "clusters" of very low δ^2H_{ms} values (Figure 6) strongly supports the idea that both δ^2H_{ms} and ^{40}Ar isotope systematics remained undisturbed after deformation. For the RRDSZ, compiled geochronological data ($^{40}Ar/^{39}Ar$ ages of biotite, muscovite, hornblende, and K-feldspar; apatite and zircon fission-track ages) point to exhumation and mid-Eocene cooling placing the Elba Quartzite in the western Raft River Mountains (Pine Creek Canyon) near the $^{40}Ar/^{39}Ar$ muscovite closure temperature isotherm prior to Miocene extension [*Wells et al.,* 2000; *Wells*, 2001]. At Pine Creek Canyon, the shapes of $^{40}Ar/^{39}Ar$ age spectra from both bulk muscovite sample (RR91-20; *Wells et al.* [2000]) and laser heating analyses of two grains (RR-04-123; this study) are remarkably similar. They show relatively young apparent ages in the initial (<10% ^{39}Ar release) heating steps, most likely due to postcrystallization ^{40}Ar loss, and a rather broad plateau over about 60–70% of total ^{39}Ar released leading to increasing apparent age steps during high-temperature gas release (Figure 5a). Such age spectra are reported from different localities in the western Raft River Mountains [e.g., *Wells et al.,* 1990, 1998, 2000].

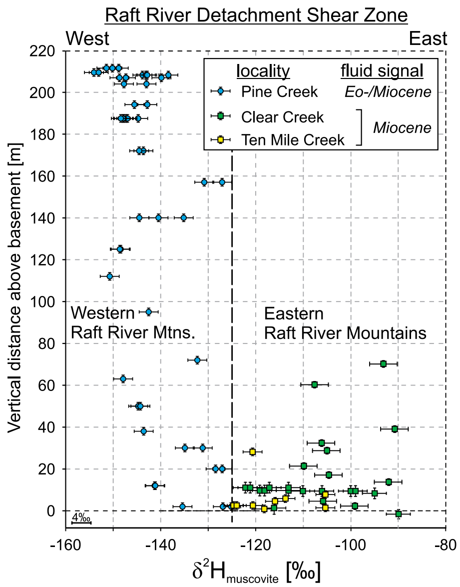

Figure 6. Comparison of δ^2H_{ms} values of white mica from Pine Creek Canyon (blue), Clear Creek Canyon (green), and Ten Mile Canyon (yellow) across the Raft River detachment shear zone. Part of the δ^2H_{ms} data of the Clear Creek Canyon is adapted from *Gottardi et al.* [2011] (see Figure 3 and supporting information).

The similarity of age spectra in both types of analysis (single grains and bulk mineral separate) shows that the general ^{39}Ar release pattern in the bulk mineral analyses is unlikely to be the result of mixed grain populations. Rather, the observed intrasample ^{40}Ar variability is due to either diffusional loss of radiogenic ^{40}Ar or intragrain recrystallization and associated resetting of the K-Ar systematics [e.g., *Mulch et al.*, 2002, 2005; *Mulch and Cosca*, 2004]. Given the oxygen isotope-based deformation temperatures (374 ± 37°C) of the RRDSZ at Pine Creek Canyon, and the roughly 5 Ma apparent age difference between quartzite that shows evidence for recrystallization and growth in the presence of very low δ^2H meteoric fluids (RR-04-123; $\delta^2H_{ms} = -151$‰) compared to the quartzite that does not (RR91-20; $\delta^2H_{ms} = -75$‰), we suggest that the deformed and crosscutting vein (RR-04-123) with a muscovite age of circa 40.4 ± 0.5 Ma most likely reflects the timing of muscovite crystallization during a late period of Eocene deformation in the presence of meteoric fluid. Thus, the vein formed during a late stage of protracted Eocene deformation that induced exhumation and cooling of the deeper segments of the RRDSZ (RR91-20).

Two new muscovite ^{40}Ar/^{39}Ar ages of 15.8 ± 0.3 Ma and 18.7 ± 0.4 Ma, together with δ^2H and δ^{18}O data from quartzite mylonite at the base of the RRDSZ at Clear Creek Canyon, delimit the end of ductile deformation in the footwall of the Raft River detachment to 16–15 Ma. The 18.7 ± 0.4 Ma age from a deformed muscovite-bearing quartz vein in mylonitic quartzite predates the formation of white mica in the highly sheared synextensional schist layer (at 8–12 m in Figure 3c) and possibly reflects vein formation or cooling during the Miocene deformation history. Together with the low δ^2H_{ms} values (−90‰ to −122‰), we interpret the 15.8 ± 0.3 Ma to reflect late-stage interaction with meteoric fluids at or near the brittle-ductile transition in the mylonitic quartzite and quartz veins, when deformation and fluid flow were localized along discrete fluid (and deformation) pathways. A 16–15 Ma deformation age is well in line with postulated middle Miocene extension and deformation along the RRDSZ at Ten Mile Canyon (~15 Ma [*Wells et al.*, 2000]) and documents the transition to brittle faulting in the upper crust and associated basin formation with deposition in the synextensional Raft River Basin starting prior to 13.5 Ma [*Konstantinou et al.*, 2012]. Collectively, these data are consistent with progressive extension-induced cooling and detachment-related exhumation by middle Miocene west-to-east unroofing along the Raft River detachment fault.

4.2. Deformation Temperatures and Development of Deformation Microstructures

At Pine Creek Canyon in the western Raft River Mountains, the limited oxygen isotope exchange thermometry data points to temperatures of 374 ± 37°C in samples that experienced interaction with very low δ^2H meteoric fluids (Figures 2 and 6). Observed deformation microstructures are consistent with two distinct temperature regimes of dislocation creep: (1) Incipient bulging recrystallization and internal deformation features, such as undulose extinction and deformation lamellae, indicative of low-temperature deformation mechanisms and temperatures of 300–400°C [*Stipp et al.*, 2002], and (2) pinning, dragging, and inclusion of small muscovite grains in quartz ribbons pointing to mobile grain boundary behavior at elevated temperatures of ~450–500°C [*Stipp et al.*, 2002]. One possible interpretation, therefore, is that Eocene (45–40 Ma) deformation of the Elba Quartzite occurred at temperatures of 374 ± 37°C and progressive exhumation and cooling of the detachment footwall established the lower temperature microstructures toward the end of Eocene extension. Alternatively, we prefer a scenario in which a lower temperature overprint (300–350°C and hence at/below the ^{40}Ar closure temperature interval) that postdates Eocene extension accounts for the seemingly distinct recrystallization regimes. In this scenario, quartz deformation features such as undulose extinction, subgrain formation, and deformation lamellae, as well as sutured grain boundaries and small grain-boundary bulges, correspond to zones of localized Miocene strain and associated fluid-rock interaction that reset muscovite hydrogen isotope compositions toward values of $\delta^2H_{ms} \geq -125‰$.

Such low Miocene temperatures and associated higher δ^2H_{fluid} values for late-stage deformation processes in the western Raft River Mountains are reasonable and agree well with the observed middle Miocene deformation temperatures at the Clear Creek Canyon and Ten Mile Canyon localities in the eastern Raft River Mountains. At these structurally deeper levels of the exhuming core complex footwall, oxygen isotope exchange temperatures within deformed Elba Quartzite show strongly compressed (140°C/100 m) isotherms with temperatures as low as 345 ± 25°C and reaching up to 485 ± 20°C at Clear Creek Canyon [*Gottardi et al.,* 2011] and 370 ± 27°C at Ten Mile Canyon, and δ^2H_{ms} values are in the range of −90‰ to −125‰ (Figure 3).

4.3. Meteoric Fluid Flow Within the Raft River Detachment System

At Pine Creek Canyon, δ^2H_{ms} values range from −125‰ to −154‰ and strongly contrast with δ^2H_{ms} values of −90 to −125‰ in the eastern Raft River Mountains at Clear Creek Canyon and Ten Mile Canyon (Figure 6). Assuming Eocene deformation temperatures of 374 ± 37°C at Pine Creek Canyon, calculated hydrogen isotope fluid compositions (δ^2H_{fluid}) (using temperature-dependent isotope fractionation coefficients from *Suzuoki and Epstein* [1976]; for a more detailed description of this calculation, see section S4 in Text S1 and Table S5 in the supporting information) for Pine Creek Canyon range between −114‰ and −126‰, whereas in the eastern Raft River Mountains δ^2H_{fluid} values range from −86‰ to −95‰ (Ten Mile Canyon; 370 ± 27°C) and from −83‰ to −103‰ (Clear Creek Canyon; assuming equilibrium temperatures between 345 and 485°C [*Gottardi et al.,* 2011]). The Pine Creek Canyon and Clear Creek Canyon/Ten Mile Canyon localities therefore document δ^2H_{fluid} values that clearly show a meteoric origin of the circulating fluids present during recrystallization and muscovite-fluid isotopic exchange [e.g., *Taylor*, 1978; *Sheppard*, 1986; *Kerrich*, 1988; *Wickham et al.,* 1993; *Mulch et al.,* 2007; *Gottardi et al.,* 2011]. However, calculated δ^2H_{fluid} values are distinctively different for Eocene (δ^2H_{fluid} values as low as −126‰) and Miocene (lowest δ^2H_{fluid} values of ~ −95‰ to −103‰) extension-related fluid-rock interaction, indicating two distinct fluid infiltration events. Both, however, require that ^2H-depleted meteoric water percolated into the uppermost levels of the detachment footwall during phases of active shearing along the detachment. This can only be achieved if, during Eocene and Miocene extension, brittle fault networks in the upper plate provided a porosity and permeability structure adequate for the downward transport of surface-derived fluids and hydraulic connectivity to actively deforming ductile footwall rocks [e.g., *Fricke et al.,* 1992; *Person et al.,* 2007].

Across the RRDSZ at Pine Creek Canyon we systematically observe intervals with increasing δ^2H_{ms} values downsection (up to −125‰; Figure 2c). This pattern might result from protracted fluid-mineral hydrogen isotope exchange extending over tens of meters downsection, which shifts the δ^2H_{fluid} of the residual fluid toward higher values, or reflects fluid flow that is coupled to more permeable layers (e.g., along muscovite rich layers) and lower δ^2H_{ms} values result from higher time-integrated fluid-rock ratios. Whatever the associated process, it is notable that the bounds to these δ^2H_{ms} data correspond to the lowest δ^2H_{ms} values of Miocene (~ −125‰) muscovites in the eastern Raft River Mountains at Clear Creek Canyon and Ten Mile Canyon (Figure 6). We therefore suggest that the observed δ^2H_{ms} pattern at Pine Creek Canyon results from pervasive Eocene (45–40 Ma) fluid-rock interaction across the entire section of Elba Quartzite with meteoric fluids that had $\delta^2H_{fluid} \geq -126‰$ and subsequent middle Miocene (18–15 Ma) overprint along discrete fluid pathways with meteoric fluids that had $\delta^2H_{fluid} \geq \sim -100‰$; an interpretation that is supported by our microstructural observations (section 4.2). The distribution of muscovite with $\delta^2H_{ms} = -132‰$ to −125‰ indicates that pathways of mid-Miocene meteoric fluids in the Pine Creek Canyon section developed at several levels across the entire thickness of Elba Quartzite and that these pathways were strongly localized within the RRDSZ. This pattern contrasts with the strongly attenuated sections of the RRDSZ in the eastern Raft River Mountains (Figures 3 and 6), where only the middle Miocene δ^2H signal is preserved in muscovite and very high strains enabled complete recrystallization of the quartzite fabric (Figure 7).

4.4. Exhumation History of the RAG-MCC

Metamorphic core complexes in the western United States have been key elements in our understanding of crustal and lithospheric deformation processes, yet despite several decades of research many aspects of their tectonic and topographic development remain controversial. Undoubtedly, Miocene Basin and Range extension played a major role in establishing the present-day architecture of crust and lithospheric mantle

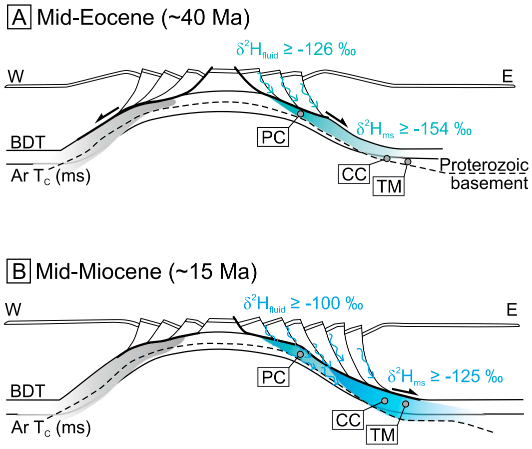

Figure 7. Tectonic models illustrating the exhumation and fluid flow history of the RAG-MCC (adapted and modified from *Wells* [2001]). Based on microstructural, $^{40}Ar/^{39}Ar$ geochronological, and stable isotopic evidence, we suggest two different exhumation and fluid infiltration events with distinct fluid compositions: (a) Mid-Eocene (45–40 Ma) exhumation and top-to-the-east shearing was accompanied by infiltration meteoric fluids with very low δ^2H values ($\delta^2H_{fluid} \geq -126‰$) resulting in δ^2H_{ms} values as low as $-154‰$, (b) Mid-Miocene extensional top-to-the-east shearing along the Raft River detachment fault led to localized hydrogen isotope exchange with meteoric water attaining δ^2H_{fluid} values of $\geq \sim -100‰$ resulting in $\delta^2H_{ms} \geq -125‰$. PC = Pine Creek; CC = Clear Creek; TM = Ten Mile Canyon. Ar T_c = Closure temperature to ^{40}Ar diffusion in muscovite; BDT = brittle-ductile transition of quartz.

underlying the Great Basin. However, there is increasing evidence that deformation structures preserved in the exhumed mylonitic footwall of MCCs may preserve geological information that dates back to earlier episodes of their tectonic history [e.g., *Wells et al.,* 1990, 2004; *Foster et al.,* 2007, 2010; *Gébelin et al.,* 2011, 2014; *Vogl et al.,* 2012; *Wong et al.,* 2013]. This also holds true for the RAG-MCC where middle to late Miocene exhumation along the RRDSZ was associated with unroofing and doming of the MCC postdating Oligocene intrusion of plutons [e.g., *Wells et al.,* 2000; *Konstantinou et al.,* 2012]. Extensional exhumation as early as the middle Eocene has been postulated to be the most likely explanation for Eocene cooling of the RAG-MCC [*Wells*, 2001] and has previously been attributed to the structurally higher top-to-the-WNW Middle Mountain shear zone [*Wells*, 2001; *Wells et al.,* 2004, 2012]. Here we expand this view and document that the east-rooted RRDSZ has a protracted history of exhuming ductile footwall rocks that started already in mid-Eocene time (45–40 Ma).

Our stable and radiogenic isotope data point to active Eocene deformation and associated fluid flow within the RRDSZ in the western Raft River Mountains. Even though we cannot determine the age of individual microstructures in the Elba Quartzite of Pine Creek Canyon, overall macroscopic and microscopic criteria indicate Eocene top-to-the-east shearing along the RRDSZ, and therefore, this zone may have been conjugate to the Eocene top-to-the-west Middle Mountain detachment fault, establishing a bivergent exhumation system (Figure 7). We partly revise previous interpretations [*Wells et al.,* 2000] that microfabric development within the western Raft River Mountains is exclusively due to low-temperature Miocene shearing along the Raft River detachment fault by documenting that (1) top-to-the-east sense of shear occurs in quartzite mylonite at the Pine Creek Canyon section, (2) white mica in these mylonites has low δ^2H_{ms} values (down to $-154‰$) that are distinct from the δ^2H values of either metamorphic muscovite or muscovite from the Elba Quartzite that experienced intense Miocene deformation and fluid-rock isotope exchange (δ^2H_{ms} between -90 and $-125‰$), and (3) $^{40}Ar/^{39}Ar$ ages of these low-δ^2H_{ms} samples indicate Eocene deformation of late-tectonic veins, fluid flow, and quartzite recrystallization in the RRDSZ, thus documenting the presence of an E-directed Eocene detachment system as early as 45–40 Ma.

The preservation of an Eocene fluid signal ($\delta^2H_{fluid} \geq -126‰$) with a Miocene overprint ($\delta^2H_{fluid} \geq \sim -100‰$) further documents that white mica-bearing fabrics in footwall mylonite of the Elba Quartzite in the western part of the Raft River Mountains were only locally affected by Miocene shearing along the RRDSZ. The Miocene RRDSZ might therefore be a reactivation and/or continuation of an Eocene top-to-the-east shear zone, suggesting that the top-to-the-WNW Middle Mountain shear zone was not the sole initiator of Eocene exhumation in the RAG-MCC. If correct, this documents an even earlier phase of bivergent core complex exhumation along two oppositely rooted detachment systems (Raft River detachment shear zone and Middle Mountain shear zone; Figure 7) in the RAG-MCC [e.g., *Malavieille and Taboada*, 1991].

5. Conclusions

Based on $^{40}Ar/^{39}Ar$ geochronological, stable isotopic, and microstructural evidence we postulate that extensional deformation along an Eocene detachment shear zone predates exhumation of mylonitic footwall rocks in the

RAG-MMC along the mid-Miocene Raft River detachment fault. Eocene extension within the Cordilleran hinterland therefore not only occurred at more northerly latitudes [e.g., *Constenius*, 1996; *Vanderhaeghe et al.,* 2003; *Foster et al.,* 2007, 2010; *Mulch et al.,* 2007] but most likely also characterized regions of the northeastern Great Basin [e.g., *Druschke et al.,* 2009; *Wells et al.,* 2012], possibly as far south as the Snake Range MCC [*Gébelin et al.,* 2014].

Eocene (circa 45–40 Ma) east-rooted detachment formation in the RAG-MCC was characterized by (1) very low δ^2H meteoric fluids ($\delta^2H_{fluid} \geq -126$‰), (2) quartzite microstructures indicative of top-to-the-east shearing under upper greenschist-facies (374 ± 37°C) conditions, and (3) (re)crystallization of white mica in synkinematic to late kinematic quartz veins at 40.4 ± 0.5 Ma. A subsequent phase of ductile extensional deformation along the Raft River detachment fault was active until the mid-Miocene (18–13 Ma) when recrystallization of low-δ^2H muscovite ended in the RRDSZ. Hydrogen isotope exchange with meteoric water ($\delta^2H_{fluid} \geq \sim -100$‰) was pervasive in the deepest (easternmost) structural levels of the exhumed RRDSZ (Ten Mile Canyon and Clear Creek Canyon).

The superposition pattern of middle Eocene and middle Miocene fluid-rock interaction within the quartzite mylonite of the RRDSZ in the western Raft River Mountains suggests that, in this region of the Miocene detachment system, localized rather than pervasive fluid flow accompanied deformation. The top-to-the-east middle Miocene extensional shearing might be a reactivation of a precursor Eocene top-to-the-east detachment shear zone in the Raft River Mountains forming a conjugate system to the middle-late Eocene to Oligocene Middle Mountain shear zone [*Saltzer and Hodges*, 1988; *Wells et al.,* 2004; *Strickland et al.,* 2011a]. Therefore, core complex exhumation along two oppositely rooted detachment systems possibly already started in Eocene times in the Raft River-Albion-Grouse Creek Mountains.

Acknowledgments
Data to support this article are available in the supporting information (Tables S1–S5). We thank M. Wong, D. A. Foster, A. Manning (USGS), and the Associate Editor for their insightful reviews that helped to significantly improve this manuscript. K.M., A.M., and A.G. acknowledge support through the LOEWE funding program of Hesse's Ministry of Higher Education, Research, and the Arts. We gratefully acknowledge support from National Science Foundation grants EAR 0838541 (CT), EAR 1019648 (CPC, AM), and EAR 0610098 (MW), as well as Swiss grants SNF-200020-126973/1 (CT) and SNF-200021-103674 (MC). We thank T. Vennemann (Lausanne) and C. Wenske (Hannover) for laboratory support. Any use of trade, product, or firm names is for descriptive purposes only and does not imply endorsement by the U.S. Government.

References

Armstrong, R. L. (1968), Sevier orogenic belt in Nevada and Utah, *Geol. Soc. Am. Bull.*, *79*(4), 429–458, doi:10.1130/0016-7606(1968)79[429:sobina]2.0.co;2.

Armstrong, R. L. (1982), Cordilleran metamorphic core complexes—From Arizona to Southern Canada, *Annu. Rev. Earth Planet. Sci.*, *10*(1), 129–154, doi:10.1146/annurev.ea.10.050182.001021.

Campani, M., A. Mulch, O. Kempf, F. Schlunegger, and N. Mancktelow (2012), Miocene paleotopography of the Central Alps, *Earth Planet. Sci. Lett.*, *337–338*, 174–185, doi:10.1016/j.epsl.2012.05.017.

Chacko, T., X. Hu, T. K. Mayeda, R. N. Clayton, and J. R. Goldsmith (1996), Oxygen isotope fractionations in muscovite, phlogopite, and rutile, *Geochim. Cosmochim. Acta*, *60*(14), 2595–2608, doi:10.1016/0016-7037(96)00112-3.

Compton, R. R. (1980), Fabrics and strains in quartzites of a metamorphic core complex Raft River Mountains, Utah, *Geol. Soc. Am. Mem.*, *153*, 385–398, doi:10.1130/MEM153-p385.

Compton, R. R., V. R. Todd, R. E. Zartman, and C. W. Naeser (1977), Oligocene and Miocene metamorphism, folding, and low-angle faulting in northwestern Utah, *Geol. Soc. Am. Bull.*, *88*(9), 1237–1250, doi:10.1130/0016-7606(1977)88<1237:oammfa>2.0.co;2.

Coney, P. J. (1980), Cordilleran metamorphic core complexes: An overview, *Geol. Soc. Am. Mem.*, *153*, 7–31, doi:10.1130/MEM153-p7.

Coney, P. J., and T. A. Harms (1984), Cordilleran metamorphic core complexes: Cenozoic extensional relics of Mesozoic compression, *Geology*, *12*(9), 550–554, doi:10.1130/0091-7613(1984)12<550:cmccce>2.0.co;2.

Constenius, K. N. (1996), Late Paleogene extensional collapse of the Cordilleran foreland fold and thrust belt, *Geol. Soc. Am. Bull.*, *108*(1), 20–39, doi:10.1130/0016-7606(1996)108<0020:lpecot>2.3.co;2.

Cosca, M., H. Stunitz, A.-L. Bourgeix, and J. P. Lee (2011), ^{40}Ar* loss in experimentally deformed muscovite and biotite with implications for ^{40}Ar/^{39}Ar geochronology of naturally deformed rocks, *Geochim. Cosmochim. Acta*, *75*(24), 7759–7778, doi:10.1016/j.gca.2011.10.012.

DeCelles, P. G. (2004), Late Jurassic to Eocene evolution of the Cordilleran thrust belt and foreland basin system, western USA, *Am. J. Sci.*, *304*(2), 105–168, doi:10.2475/ajs.304.2.105.

Dickinson, W. R. (2002), The basin and range province as a composite extensional domain, *Int. Geol. Rev.*, *44*(1), 1–38, doi:10.2747/0020-6814.44.1.1.

Drury, M. R., and J. L. Urai (1990), Deformation-related recrystallization processes, *Tectonophysics*, *172*(3–4), 235–253, doi:10.1016/0040-1951(90)90033-5.

Druschke, P., A. D. Hanson, and M. L. Wells (2009), Structural, stratigraphic, and geochronologic evidence for extension predating Palaeogene volcanism in the Sevier hinterland, east-central Nevada, *Int. Geol. Rev.*, *51*(7–8), 743–775, doi:10.1080/00206810902917941.

Egger, A. E., T. A. Dumitru, E. L. Miller, C. F. I. Savage, and J. L. Wooden (2003), Timing and nature of tertiary plutonism and extension in the Grouse Creek Mountains, Utah, *Int. Geol. Rev.*, *45*(6), 497–532, doi:10.2747/0020-6814.45.6.497.

Famin, V., P. Philippot, L. Jolivet, and P. Agard (2004), Evolution of hydrothermal regime along a crustal shear zone, Tinos Island, Greece, *Tectonics*, *23*(5), TC5004, doi:10.1029/2003TC001509.

Foster, D. A., P. T. Doughty, T. J. Kalakay, C. M. Fanning, S. Coyner, W. C. Grice, and J. Vogl (2007), Kinematics and timing of exhumation of metamorphic core complexes along the Lewis and Clark fault zone, northern Rocky Mountains USA, *Geol. Soc. Am. Spec. Pap.*, *434*, 207–232, doi:10.1130/2007.2434(10).

Foster, D. A., W. C. Grice, and T. J. Kalakay (2010), Extension of the Anaconda metamorphic core complex: ^{40}Ar/^{39}Ar thermochronology and implications for Eocene tectonics of the northern Rocky Mountains and the Boulder batholith, *Lithosphere*, *2*(4), 232–246, doi:10.1130/l94.1.

Fricke, H. C., S. M. Wickham, and J. R. O'Neil (1992), Oxygen and hydrogen isotope evidence for meteoric water infiltration during mylonitization and uplift in the Ruby Mountains-East Humboldt Range core complex Nevada, *Contrib. Mineral. Petrol.*, *111*, 203–221, doi:10.1007/BF00348952.

Gébelin, A., A. Mulch, C. Teyssier, M. Heizler, T. Vennemann, and N. C. A. Seaton (2011), Oligo-Miocene extensional tectonics and fluid flow across the Northern Snake Range detachment system, Nevada, *Tectonics*, *30*, TC5010, doi:10.1029/2010TC002797.

Gébelin, A., A. Mulch, C. Teyssier, C. Page Chamberlain, and M. Heizler (2012), Coupled basin-detachment systems as paleoaltimetry archives of the western North American Cordillera, *Earth Planet. Sci. Lett.*, *335–336*, 36–47, doi:10.1016/j.epsl.2012.04.029.

Gébelin, A., A. Mulch, C. Teyssier, M. J. Jessup, R. D. Law, and M. Brunel (2013), The Miocene elevation of Mount Everest, *Geology*, doi:10.1130/g34331.1.

Gébelin, A., C. Teyssier, M. Heizler, and A. Mulch (2014), Meteoric water circulation in a rolling-hinge detachment system (northern Snake Range core complex, Nevada), *Geol. Soc. Am. Bull.*, *127*(1–2), 149–161, doi:10.1130/b31063.1.

Gottardi, R., and C. Teyssier (2013), Thermomechanics of an extensional shear zone, Raft River metamorphic core complex, NW Utah, *J. Struct. Geol.*, *53*, 54–69, doi:10.1016/j.jsg.2013.05.012.

Gottardi, R., C. Teyssier, A. Mulch, T. W. Vennemann, and M. L. Wells (2011), Preservation of an extreme transient geotherm in the Raft River detachment shear zone, *Geology*, *39*(8), 759–762, doi:10.1130/g31834.1.

Gottardi, R., C. Teyssier, A. Mulch, J. W. Valley, M. J. Spicuzza, T. W. Vennemann, A. Quilichinni, and M. Heizler (2015), Strain and permeability gradients traced by stable isotope exchange in the Raft River detachment shear zone, Utah, *J. Struct. Geol.*, *71*, 41–57, doi:10.1016/j.jsg.2014.10.005.

Harrison, T. M., J. Célérier, A. B. Aikman, J. Hermann, and M. T. Heizler (2009), Diffusion of ^{40}Ar in muscovite, *Geochim. Cosmochim. Acta*, *73*(4), 1039–1051, doi:10.1016/j.gca.2008.09.038.

Hetzel, R., H. Zwingmann, A. Mulch, K. Gessner, C. Akal, A. Hampel, T. Güngör, R. Petschick, T. Mikes, and F. Wedin (2013), Spatiotemporal evolution of brittle normal faulting and fluid infiltration in detachment fault systems: A case study from the Menderes Massif, western Turkey, *Tectonics*, *32*, 364–376, doi:10.1002/tect.20031.

Hoisch, T. D., M. L. Wells, and L. M. Hanson (2002), Pressure-temperature paths from garnet-zoning: Evidence for multiple episodes of thrust burial in the hinterland of the Sevier orogenic belt, *Am. Mineral.*, *87*(1), 115–131.

Jessell, M. W. (1987), Grain-boundary migration microstructures in a naturally deformed quartzite, *J. Struct. Geol.*, *9*(8), 1007–1014, doi:10.1016/0191-8141(87)90008-3.

Kerrich, R. (1988), Detachment zones of Cordilleran metamorphic core complexes: Thermal, fluid and metasomatic regimes, *Geol. Rundsch.*, *77*(1), 157–182, doi:10.1007/bf01848682.

Konstantinou, A., A. Strickland, E. L. Miller, and J. P. Wooden (2012), Multistage Cenozoic extension of the Albion–Raft River–Grouse Creek metamorphic core complex: Geochronologic and stratigraphic constraints, *Geosphere*, *8*(6), 1429–1466, doi:10.1130/ges00778.1.

Konstantinou, A., A. Strickland, E. Miller, J. Vervoort, C. M. Fisher, J. Wooden, and J. Valley (2013), Synextensional magmatism leading to crustal flow in the Albion–Raft River–Grouse Creek metamorphic core complex, northeastern Basin and Range, *Tectonics*, *32*, 1384–1403, doi:10.1002/tect.20085.

Lister, G. S., and A. W. Snoke (1984), S-C mylonites, *J. Struct. Geol.*, *6*(6), 617–638, doi:10.1016/0191-8141(84)90001-4.

Malavieille, J. (1987), Kinematics of compressional and extensional ductile shearing deformation in a metamorphic core complex of the northeastern Basin and Range, *J. Struct. Geol.*, *9*(5–6), 541–554, doi:10.1016/0191-8141(87)90139-8.

Malavieille, J., and A. Taboada (1991), Kinematic model for postorogenic Basin and Range extension, *Geology*, *19*(6), 555–558, doi:10.1130/0091-7613(1991)019<0555:kmfpba>2.3.co;2.

Manning, A. H., and J. M. Bartley (1994), Postmylonitic deformation in the Raft River metamorphic core complex, northwestern Utah: Evidence of a rolling hinge, *Tectonics*, *13*(3), 596–612, doi:10.1029/93TC03321.

McFadden, R. R., A. Mulch, C. Teyssier, N. C. Seaton, and L. Tokle (2010), The relationship between microstructure and hydrogen isotopes in the Wildhorse detachment, Pioneer Mountains, Idaho, Abstract #T41B-2152 presented at 2010 Fall Meeting, AGU, San Francisco, Calif.

Menzies, C. D., D. A. H. Teagle, D. Craw, S. C. Cox, A. J. Boyce, C. D. Barrie, and S. Roberts (2014), Incursion of meteoric waters into the ductile regime in an active orogen, *Earth Planet. Sc. Lett.*, *399*, 1–13, doi:10.1016/j.epsl.2014.04.046.

Miller, E. L., A. Konstantinou, and A. Strickland (2012), Comment on "Geodynamics of synconvergent extension and tectonic mode switching: Constraints from the Sevier-Laramide orogen" by Michael L. Wells et al., *Tectonics*, *31*, TC4015, doi:10.1029/2012TC003103.

Morrison, J., and J. L. Anderson (1998), Footwall refrigeration along a detachment fault: Implications for the thermal evolution of core complexes, *Science*, *279*(5347), 63–66, doi:10.1126/science.279.5347.63.

Mulch, A., and C. P. Chamberlain (2007), Stable isotope paleoaltimetry in orogenic belts—The silicate record in surface and crustal geological archives, *Rev. Mineral. Geochem.*, *66*(1), 89–118, doi:10.2138/rmg.2007.66.4.

Mulch, A., and M. A. Cosca (2004), Recrystallization or cooling ages: In situ UV-laser ^{40}Ar/^{39}Ar geochronology of muscovite in mylonitic rocks, *J. Geol. Soc. London*, *161*(4), 573–582, doi:10.1144/0016-764903-110.

Mulch, A., M. A. Cosca, and M. Handy (2002), In-situ UV-laser ^{40}Ar/^{39}Ar geochronology of a micaceous mylonite: An example of defect-enhanced argon loss, *Contrib. Mineral. Petrol.*, *142*(6), 738–752, doi:10.1007/s00410-001-0325-6.

Mulch, A., C. Teyssier, M. A. Cosca, O. Vanderhaeghe, and T. W. Vennemann (2004), Reconstructing paleoelevation in eroded orogens, *Geology*, *32*(6), 525–528, doi:10.1130/g20394.1.

Mulch, A., M. A. Cosca, A. Andresen, and J. Fiebig (2005), Time scales of deformation and exhumation in extensional detachment systems determined by high-spatial resolution in situ UV-laser ^{40}Ar/^{39}Ar dating, *Earth Planet. Sci. Lett.*, *233*(3–4), 375–390, doi:10.1016/j.epsl.2005.01.042.

Mulch, A., C. Teyssier, M. A. Cosca, and T. W. Vennemann (2006), Thermomechanical analysis of strain localization in a ductile detachment zone, *J. Geophys. Res.*, *111*, B12405, doi:10.1029/2005JB004032.

Mulch, A., C. Teyssier, M. A. Cosca, and C. P. Chamberlain (2007), Stable isotope paleoaltimetry of Eocene core complexes in the North American Cordillera, *Tectonics*, *26*, TC4001, doi:10.1029/2006TC001995.

Person, M., A. Mulch, C. Teyssier, and Y. Gao (2007), Isotope transport and exchange within metamorphic core complexes, *Am. J. Sci.*, *307*(3), 555–589, doi:10.2475/03.2007.01.

Rey, P. F., C. Teyssier, and D. L. Whitney (2009), Extension rates, crustal melting, and core complex dynamics, *Geology*, *37*(5), 391–394, doi:10.1130/g25460a.1.

Saltzer, S. D., and K. V. Hodges (1988), The Middle Mountain shear zone, southern Idaho: Kinematic analysis of an early Tertiary high-temperature detachment, *Geol. Soc. Am. Bull.*, *100*(1), 96–103, doi:10.1130/0016-7606(1988)100<0096:tmmszs>2.3.co;2.

Sheely, J. C., M. L. Wells, and T. L. Spell (2001), Timing and kinematics of an Eocene-Miocene shear zone: Grouse Creek Mountains, Utah, *Geol. Soc. Am. Abstr. Programs*, *33*(6), 148.

Sheppard, S. M. F. (1986), Characterization and isotopic variations in natural waters, *Rev. Mineral. Geochem.*, *16*(1), 165–183.

Simpson, C., and S. M. Schmid (1983), An evaluation of criteria to deduce the sense of movement in sheared rocks, *Geol. Soc. Am. Bull.*, *94*(11), 1281–1288, doi:10.1130/0016-7606(1983)94<1281:aeoctd>2.0.co;2.

Sonder, L. J., and C. H. Jones (1999), Western United States extension: How the West was widened, *Annu. Rev. Earth Planet. Sci.*, *27*(1), 417–462, doi:10.1146/annurev.earth.27.1.417.

Stipp, M., H. Stünitz, R. Heilbronner, and S. M. Schmid (2002), The eastern Tonale fault zone: A 'natural laboratory' for crystal plastic deformation of quartz over a temperature range from 250 to 700°C, *J. Struct. Geol.*, *24*(12), 1861–1884, doi:10.1016/S0191-8141(02)00035-4.

Strickland, A., E. L. Miller, and J. L. Wooden (2011a), The timing of Tertiary metamorphism and deformation in the Albion–Raft River–Grouse Creek metamorphic core complex, Utah and Idaho, *J. Geol.*, *119*(2), 185–206, doi:10.1086/658294.

Strickland, A., E. L. Miller, J. L. Wooden, R. Kozdon, and J. W. Valley (2011b), Syn-extensional plutonism and peak metamorphism in the Albion–Raft River–Grouse Creek metamorphic core complex, *Am. J. Sci.*, *311*(4), 261–314, doi:10.2475/04.2011.01.

Sullivan, W. A. (2008), Significance of transport-parallel strain variations in part of the Raft River shear zone, Raft River Mountains, Utah, USA, *J. Struct. Geol.*, *30*(2), 138–158, doi:10.1016/j.jsg.2007.11.007.

Sullivan, W. A., and A. W. Snoke (2007), Comparative anatomy of core-complex development in the northeastern Great Basin, U.S.A, *Rocky Mt. Geol.*, *42*(1), 1–29, doi:10.2113/gsrocky.42.1.1.

Suzuoki, T., and S. Epstein (1976), Hydrogen isotope fractionation between OH-bearing minerals and water, *Geochim. Cosmochim. Acta*, *40*(10), 1229–1240, doi:10.1016/0016-7037(76)90158-7.

Taylor, H. P., Jr. (1978), Oxygen and hydrogen isotope studies of plutonic granitic rocks, *Earth Planet. Sci. Lett.*, *38*(1), 177–210, doi:10.1016/0012-821X(78)90131-0.

Teyssier, C., E. C. Ferré, D. L. Whitney, B. Norlander, O. Vanderhaeghe, and D. Parkinson (2005), Flow of partially molten crust and origin of detachments during collapse of the Cordilleran orogen, *Geol. Soc., London, Spec. Publ.*, *245*(1), 39–64, doi:10.1144/gsl.sp.2005.245.01.03.

Vanderhaeghe, O., C. Teyssier, I. McDougall, and W. J. Dunlap (2003), Cooling and exhumation of the Shuswap Metamorphic Core Complex constrained by $^{40}Ar/^{39}Ar$ thermochronology, *Geol. Soc. Am. Bull.*, *115*(2), 200–216, doi:10.1130/0016-7606(2003)115<0200:caeots>2.0.co;2.

Vogl, J. J., D. A. Foster, C. M. Fanning, K. A. Kent, D. W. Rodgers, and T. Diedesch (2012), Timing of extension in the Pioneer metamorphic core complex with implications for the spatial-temporal pattern of Cenozoic extension and exhumation in the northern U.S. Cordillera, *Tectonics*, *31*, TC1008, doi:10.1029/2011TC002981.

Wells, M. L. (1997), Alternating contraction and extension in the hinterlands of orogenic belts: An example from the Raft River Mountains, Utah, *Geol. Soc. Am. Bull.*, *109*(1), 107–126, doi:10.1130/0016-7606(1997)109<0107:acaeit>2.3.co;2.

Wells, M. L. (2001), Rheological control on the initial geometry of the Raft River detachment fault and shear zone, western United States, *Tectonics*, *20*(4), 435–457, doi:10.1029/2000TC001202.

Wells, M. L., and T. D. Hoisch (2012), Reply to comment by E. L. Miller et al. on "Geodynamics of synconvergent extension and tectonic mode switching: Constraints from the Sevier-Laramide orogen", *Tectonics*, *31*, TC4016, doi:10.1029/2012TC003136.

Wells, M. L., R. D. Dallmeyer, and R. W. Allmendinger (1990), Late Cretaceous extension in the hinterland of the Sevier thrust belt, northwestern Utah and southern Idaho, *Geology*, *18*(10), 929–933, doi:10.1130/0091-7613(1990)018<0929:lceith>2.3.co;2.

Wells, M. L., T. D. Hoisch, M. T. Peters, D. M. Miller, E. D. Wolff, and L. M. Hanson (1998), The Mahogany Peaks fault, a Late Cretaceous-Paleocene(?) Normal fault in the Hinterland of the Sevier Orogen, *J. Geol.*, *106*(5), 623–634, doi:10.1086/516046.

Wells, M. L., L. W. Snee, and A. E. Blythe (2000), Dating of major normal fault systems using thermochronology: An example from the Raft River detachment, Basin and Range, western United States, *J. Geophys. Res.*, *105*(B7), 16,303–16,327, doi:10.1029/2000JB900094.

Wells, M. L., J. C. Sheeley, T. L. Spell, E. D. Kelly, and T. D. Hoisch (2004), Eocene extension in northwestern Utah-southern Idaho: Early motion on the polyphase Middle Mountain shear zone, Rocky Mountain (56th Annual) and Cordilleran (100th Annual) Joint Meeting (May 3–5, 2004).

Wells, M. L., T. D. Hoisch, A. M. Cruz-Uribe, and J. D. Vervoort (2012), Geodynamics of synconvergent extension and tectonic mode switching: Constraints from the Sevier-Laramide orogen, *Tectonics*, *31*, TC1002, doi:10.1029/2011TC002913.

Wernicke, B. (1981), Low-angle normal faults in the Basin and Range Province: Nappe tectonics in an extending orogen, *Nature*, *291*(5817), 645–648, doi:10.1038/291645a0.

Whitney, D. L., C. Teyssier, P. Rey, and W. R. Buck (2013), Continental and oceanic core complexes, *Geol. Soc. Am. Bull.*, *125*(3/4), 273–298, doi:10.1130/b30754.1.

Wickham, S. M., M. T. Peters, H. C. Fricke, and J. R. O'Neil (1993), Identification of magmatic and meteoric fluid sources and upward- and downward-moving infiltration fronts in a metamorphic core complex, *Geology*, *21*(1), 81–84, doi:10.1130/0091-7613(1993)021<0081:iomamf>2.3.co;2.

Wong, M. S., J. Singleton, J. Baughman, and K. C. Bunting (2013), Evidence for Miocene reactivation of a late Cretaceous to early Tertiary shear zone in the Harcuvar and Buckskin-rawhide metamorphic core complexes, Arizona, in *2013 GSA Annual Meeting in Denver: 125th Anniversary of GSA (27–30 October 2013)*, pp. 523, Geol. Soc. of Am., Denver.